

Konrad Szymański\*, Paweł Moskał, Tomasz Bednarski, Piotr Białas, Eryk Czerwiński, Krzysztof Giergiel, Łukasz Kapłon, Andrzej Kochanowski, Grzegorz Korcyl, Jakub Kowal, Paweł Kowalski, Tomasz Kozik, Wojciech Krzemień, Marcin Molenda, Ines Moskał, Szymon Niedźwiecki, Marek Pałka, Monika Pawlik-Niedźwiecka, Lech Raczyński, Zbigniew Rudy, Piotr Salabura, Neha Sharma, Michał Silarski, Artur Słomski, Jerzy Smyrski, Adam Strzelecki, Piotr Witkowski, Wojciech Wiślicki, Marcin Zieliński and Natalia Zoń

# Simulations of $\gamma$ quanta scattering in a single module of the J-PET detector

**Abstract:** This article describes the simulations of the scattering of annihilation  $\gamma$  quanta in a strip of a plastic scintillator. Such strips constitute the basic detection modules in a newly proposed positron emission tomography (PET), which utilizes plastic scintillators instead of inorganic crystals. An algorithm simulating the chain of Compton scatterings was elaborated and a series of simulations have been conducted for the scintillator strip with a cross-section of  $5 \times 19$  mm. The results indicate that secondary interactions occur only in the case of about 8% of the events and only 25% of these events take place in the distance larger than 0.5 cm from the primary interaction. Also, the light signals produced at the primary and secondary interactions overlap with the delay, the distribution of which is characterized by a full width at half-maximum (FWHM) of about 40 ps.

**Keywords:** Compton scattering; Monte Carlo simulation; time-of-flight positron emission tomography.

\*Corresponding author: Konrad Szymański, Institute of Physics, Jagiellonian University, 30-059 Cracow, Poland, E-mail: konrad.szymanski@uj.edu.pl

Paweł Moskał, Tomasz Bednarski, Piotr Białas, Eryk Czerwiński, Krzysztof Giergiel, Grzegorz Korcyl, Jakub Kowal, Tomasz Kozik, Wojciech Krzemień, Ines Moskał, Szymon Niedźwiecki, Marek Pałka, Monika Pawlik-Niedźwiecka, Zbigniew Rudy, Piotr Salabura, Neha Sharma, Michał Silarski, Artur Słomski, Jerzy Smyrski, Adam Strzelecki, Piotr Witkowski, Marcin Zieliński and Natalia Zoń: Institute of Physics, Jagiellonian University, 30-059 Cracow, Poland  
Łukasz Kapłon: Institute of Physics, Jagiellonian University, 30-059 Cracow, Poland; and Faculty of Chemistry, Jagiellonian University, 30-060 Cracow, Poland

Andrzej Kochanowski and Marcin Molenda: Faculty of Chemistry, Jagiellonian University, 30-060 Cracow, Poland

Paweł Kowalski, Lech Raczyński and Wojciech Wiślicki: Świerk Computing Centre, National Centre for Nuclear Research, 05-400 Otwock-Świerk, Poland

## Introduction

Recently, a novel solution for the positron emission tomography (PET) scanner was proposed, which utilizes plastic scintillators as the detectors for the annihilation quanta [1]. A single detection unit of this detector is built out of a scintillator strip read out on both sides by photomultipliers. The position of the interaction of the  $\gamma$  quanta inside a strip is determined based on the shape and time of the photomultiplier signals. The shape of the signals may be distorted by the secondary scattering of the  $\gamma$  quanta inside the scintillator. This is because a secondary scattering creates an additional light signal, and as a result, a light pulse reaching the photomultiplier is composed of overlapping signals originating from the points of primary and secondary interactions.

In this article, we estimate the influence of the secondary scattering on the quality of hit position reconstruction in the PET detectors based on the plastic scintillators. To this end, a dedicated simulation program was elaborated and a series of simulations have been performed. These allowed to determine the multiplicity distributions of the annihilation quanta interaction inside a scintillator strip as well as the distributions of the distance between the points of scattering. The results are then interpreted in view of the distortion of the spatial and temporal resolution of the detector due to the secondary interactions of the registered  $\gamma$  quanta. The main simulation algorithm is elaborated assuming that in plastic scintillators the annihilation  $\gamma$  quanta with energy of about 511 keV undergo a Compton scattering only.

## Algorithm

The main aim of the simulation was an estimation of the number of  $\gamma$  quanta interactions in a scintillator strip and

the determination of the spatial distribution of scattering centers within the scintillator volume. For this purpose, we assume that  $\gamma$  quantum originates in a certain initial position with a user-defined four-momentum vector. The description of scintillator is also provided by the user and consists of the attenuation constant at energy for 511 keV and the dimensions of scintillator cuboid. From this input data, the attenuation constant at any energy is extrapolated using the following formula:

$$\lambda(E) = \frac{\sigma(E)}{\sigma(E_0)} \lambda(E_0), \quad (1)$$

where  $\lambda$  denotes the inverse of the attenuation length and  $\sigma$  stands for the total cross-section of  $\gamma$  quantum at a given energy  $E$ . The values of the cross-sections have been extracted from [2]. A given number of events  $N$  and a maximum number of interactions in one event  $k$  are also passed to the algorithm, which may be in general described by the following scheme:

```

while number of events  $\leq N$  do
  position  $\leftarrow$  initial position
  direction  $\leftarrow$  initial direction
  energy  $\leftarrow$  initial energy
  while number of interactions  $\leq k$  do
     $\lambda \leftarrow ne \cdot$  total cross-section
    length  $\leftarrow$  random length of probability density function (PDF)  $\rho(x>0) = \lambda \exp(-x\lambda)$ 
    position  $\leftarrow$  position + direction  $\cdot$  length
    if position not in scintillator, then
      end event
    end if
    polar angle  $\leftarrow$  random angle from Klein-Nishina PDF
    azimuthal angle  $\leftarrow$  random angle from isotropic PDF
    "scatter" direction vector using generated angles
    print position, deposited energy, time
  end while
end while

```

As a result, the collection of events containing an ordered set of interactions is obtained.

## Generating random data from the desired PDF

The generation of variables used in the program according to the given PDF is performed based on the distribution of a corresponding cumulative function, which is homogeneous by definition. The cumulative function ( $D(\theta)$ ) of the angular PDF is calculated based on the Klein-Nishina formula [3]. In the following equations, it is factorized into

$\theta$ -independent (constant  $C$ ) and  $\theta$ -dependent functions, and the other  $\theta$ -independent function is added (only the relative changes to  $D(\theta)$  are important; the additive function is chosen to ensure that  $D(\theta)=0$ , which simplifies the calculations):

$$D(\theta) = C \cdot [(-5\gamma^2 + 2(2\gamma+1)\gamma \cos\theta - 6\gamma - 2)P^2(\theta, \gamma) + 2(\gamma^2 - 2\gamma - 2) \ln\left(\frac{1}{P(\theta, \gamma)}\right) - 2\gamma \cos\theta]$$

$$P(\theta, \gamma) = \frac{1}{1 + \gamma(1 - \cos\theta)}$$

$$\gamma = \frac{E}{m_e c^2},$$

where  $E$  denotes the energy of  $\gamma$  quantum and  $m_e$  stands for the mass of electron.

This method is used only for the generation of scattering angle  $\theta$ . In the case of the distance  $l$  between subsequent scatterings, a cumulative distribution function can be derived analytically since the PDF possesses an exponential form:

$$P(l) = \frac{1}{\lambda} \exp(-\lambda l) \quad (2)$$

where  $l \geq 0$ . Hence, cumulative function reads

$$D(l) = 1 - \exp(-\lambda l). \quad (3)$$

Therefore, for a given random number of uniform distribution  $r \in [0, 1]$ ,

$$l = -\frac{\ln(1-r)}{\lambda}. \quad (4)$$

## A method of simulation of $\gamma$ quanta scattering

In order to effectively simulate a series of scatterings, we have elaborated an algorithm in which the calculations reduce to the rotations of vectors. For given vector  $v \in \mathbb{R}^3$ , the rotation matrix  $O_1$  ( $O$ -matrices are changing the reference frame, while  $S$ -matrices describe the transformation of the vector in a particular frame) fulfilling the condition

$$O_1 \cdot v = \begin{bmatrix} 0 \\ v'_2 \\ v'_3 \end{bmatrix}$$

is generated. Let  $O_1 \cdot v = v'$ . Then, another rotation matrix  $O_2$ , such that

$$v'' = O_2 \cdot v' = \begin{bmatrix} 0 \\ 0 \\ v''_3 \end{bmatrix}$$

is computed. Now, the scattering can be simulated by the rotation of vector  $v''$  by means of matrix  $S_1$  in such way that  $S_1 \cdot v''$  forms a desired angle with z-axis. To preserve the cylindrical symmetry, this vector must be rotated by a rotation matrix around the z-axis  $S_2$  by a random angle. The generated vector must be retransformed to the original reference frame, and the final scattered vector is given by

$$v_{\text{scatt}} = O_1^{-1} O_2^{-1} S_2 S_1 O_2 O_1 v.$$

The discussed rotations are visualized in Figure 1.

## Validation of the algorithm assumptions

The  $\gamma$  quantum passing through the matter may undergo various processes, among which the Compton, Rayleigh, and photoelectric effects are dominant for the energy range below 1 MeV. For the simulations of the interaction of annihilation quanta in a plastic scintillator, we assumed the dominance of the Compton effect and have neglected the other processes, since they can contribute significantly only for energies below 50 keV (see Figure 2).

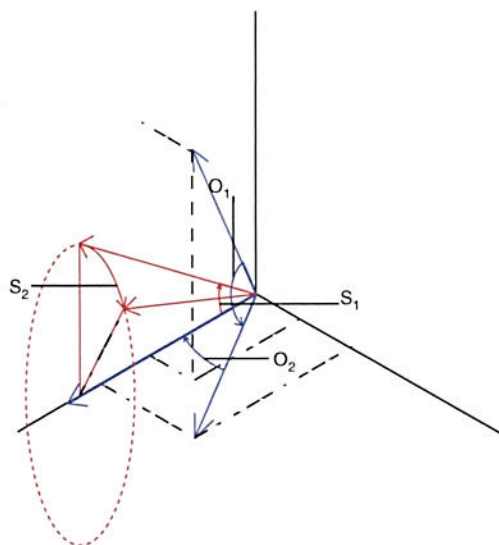


**Figure 1** Pictorial presentation of vector rotations applied for the simulations of the Compton scattering.

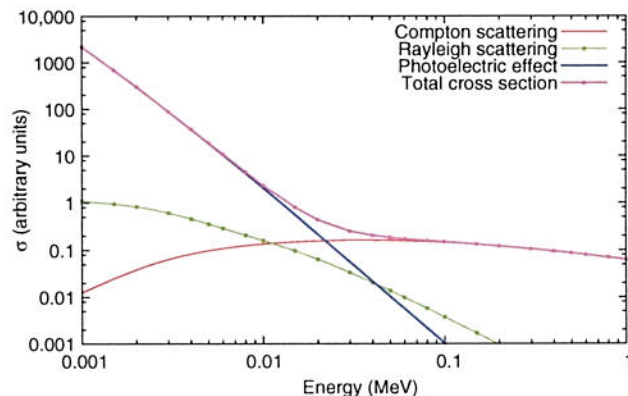


**Figure 2** Total cross-sections of the various effects for  $\gamma$  quanta scattering in carbon as a function of energy [2].

The energy of a  $\gamma$  quantum may be expressed in terms of the “reduced  $\gamma$  quantum energy”  $\gamma = \frac{h\nu}{m_e c^2}$ . Such notation is especially convenient for the calculations involving annihilation quanta for which  $\gamma=1$ . For a further consideration, it is useful to mention that  $\gamma \approx 0.1$  for  $\gamma$  quantum with an energy of 50 keV.

In the scintillator strip, the annihilation  $\gamma$  quantum may in principle undergo many Compton scatterings and its minimum energy after the  $n$ th interaction may be calculated based on the iterative formula:

$$\gamma_{n+1} = \frac{\gamma_n}{1 + 2\gamma_n} \quad (5)$$

The first terms of this series are (1, 0.33, 0.19, 0.14, 0.11, 0.09, K). It shows that up to the fourth interaction energy of  $\gamma$  quantum is above 50 keV. It will be shown in the following sections that, in the case of the scintillator strips of the J-PET detector, a probability that the  $\gamma$  quantum scatters more than three times is negligible. Therefore, all effects other than the Compton scattering can be safely neglected.

Another assumption applied is the convexity of scintillator’s shape: in such case, if  $\gamma$  quantum leaves the scintillator, it will never come back and the computations can stop. It is also certain (from the definition) that the line segment bounded by two points of interactions is inside the scintillator’s volume, which simplifies the calculations of the next interaction point.

## Results

We have performed the simulations assuming that the scintillator strip is a cuboid with dimensions of

200×0.5×2 cm (see Figure 3). The cross-section of the strip corresponds to the size of the modules used for the first J-PET prototype, and its length was chosen arbitrarily large. The starting point of  $\gamma$  quanta was placed on the middle of a 2000×0.5 cm wall. Its initial energy was set to  $m_e c^2 \approx 511$  keV ( $\gamma=1$ ). The number  $k$  was set to 1000 to make sure that all possible interactions were taken into account. The simulations were performed for the three directions of the  $\gamma$  quanta as shown in Figure 2. The three cases denoted in Figure 2 as A–C have initial direction vectors of (0,0,-1), (0,-1,-1), and (-1,0,-1), respectively. For each direction,  $10^6$  events were simulated. The attenuation constant (derived from the information in [4] for BC-408, BC-420, and BC-422 scintillators and [2]) at  $\gamma=1$  was set to  $0.1 \text{ cm}^{-1}$ .

### Multiplicity of the interactions

The distribution of the multiplicity of interactions determined for the three studied directions A–C is shown in Table 1.

The result in this table indicates that only in about 8% of the events the  $\gamma$  quantum scatters more than once inside the scintillator strip.

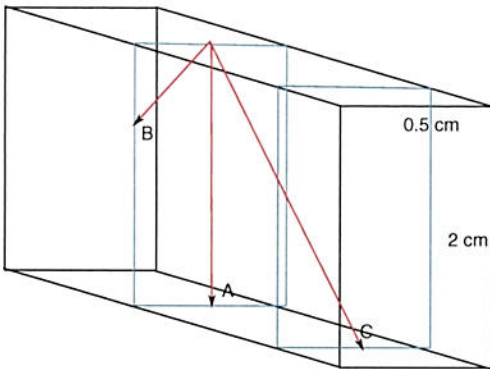


**Figure 3** Graphical presentation of the simulation conditions. Red lines show the initial direction of flight of  $\gamma$  quanta for cases A–C.

**Table 1** Frequency of occurrence of interactions.

Level	Frequency (A)	Frequency (B)	Frequency (C)
1	100%	100%	100%
2	7.9%	5.7%	8.3%
3	0.66%	0.44%	0.71%
4	0.06%	0.04%	0.07%

The frequency of level  $k$  indicates the fraction of events with  $k$  or more number of interactions. The values are obtained by taking into account only these events for which  $\gamma$  quantum interacted in the scintillator.

### Spatial distribution of the interaction points

The points of the primary interaction populates a line along the direction of the flight of the  $\gamma$  quantum with the density decreasing exponentially with a distance from a point of emission. This decrease is governed by the attenuation length, which for the plastic scintillator and annihilation  $\gamma$  quanta amounts to about 10 cm [4]. The distribution of the distances between the consecutive interaction points is more complicated to describe because the energy and hence the attenuation length of scattered  $\gamma$  quanta varies from event to event. It can be, however, estimated numerically based on the simulations described in this article. The most relevant for the reconstruction of the hit position along the scintillator strip is a difference ( $\Delta x$ ) of  $x$ -coordinates between the primary and secondary interaction points. The  $x$ -direction is the one along the largest dimension of a scintillator strip.

The greater the  $|\Delta x|$  is, the more blurred is the signal from the photomultiplier. A full width at half-maximum (FWHM) of this distribution is rather small [ $\text{FWHM}(|\Delta x|) \approx 0.3 \text{ cm}$ , see Figure 4]. However, since the distribution has a long tail, it is useful to tabularize its quantiles (see Table 2).

Table 2 indicates that more than 90% of secondary scattering occurs for  $|\Delta x|$  smaller than 1.4 cm. However, for

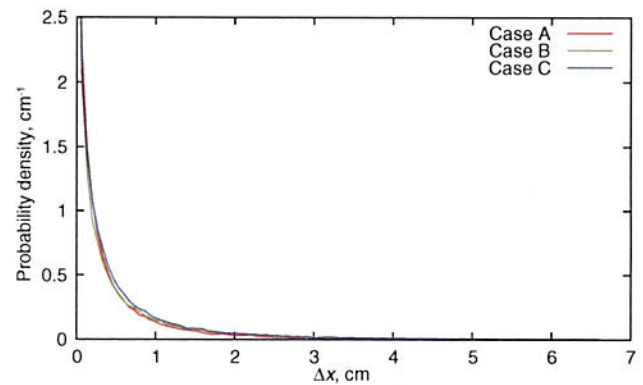


**Figure 4** PDFs of  $|\Delta x|$  defined as a distance along the scintillator between the primary and secondary interaction points.

**Table 2** Quantiles of  $|\Delta x|$  distribution as shown in Figure 4.

Quantile	Case A (cm)	Case B (cm)	Case C (cm)
0.25	0.042	0.035	0.060
0.50	0.16	0.16	0.21
0.75	0.46	0.54	0.61
0.90	1.1	1.3	1.4
0.95	1.7	2.1	2.2
0.99	3.5	3.8	3.9

the distortion of the signals, not only a distance between the interaction points is important but also the energy deposited by the secondary ionization.

### Energy deposition versus the spatial separation of interaction points

The correlations between the deposited energy and spatial separation of interaction points is shown in Figures 5–7. These figures are, however, not 2D histograms (i.e., heat maps) but sets of densely packed 1D histograms, in which each line (subhistogram) is separately normalized in the way that the maximum value in each subhistogram is equal to 1. The figures are made this way, because one may approximate the total energy stored in scintillator and could be interested in the most probable  $|\Delta x|$  in this event. It is important to mention that, in this and the following paragraphs, only the events including at least two scatterings were taken into account.

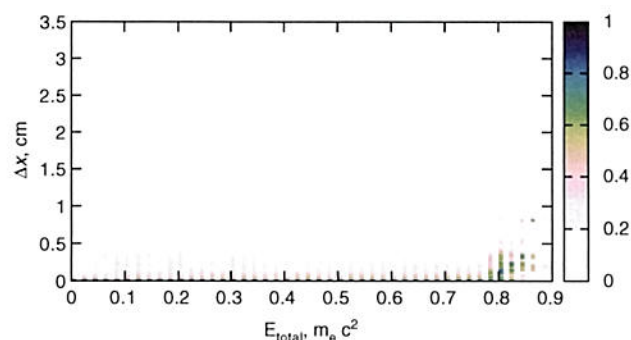


**Figure 5** Case A: histograms of  $|\Delta x|$  as a function of total deposited energy.

This figure shows a set of 1D histograms normalized to unity in maximum. A more detailed description can be found in the text.

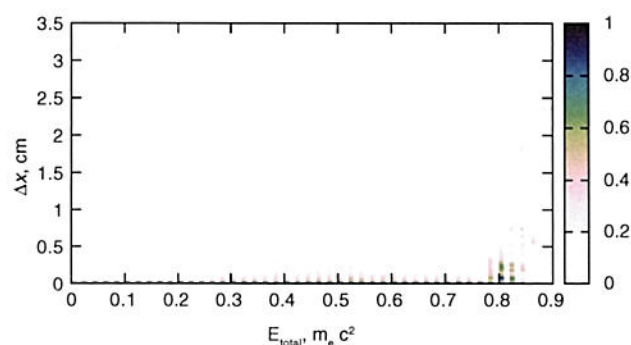


**Figure 6** Case B: histograms of  $|\Delta x|$  as a function of total deposited energy.

This figure shows a set of 1D histograms normalized to unity in maximum. A more detailed description can be found in the text.

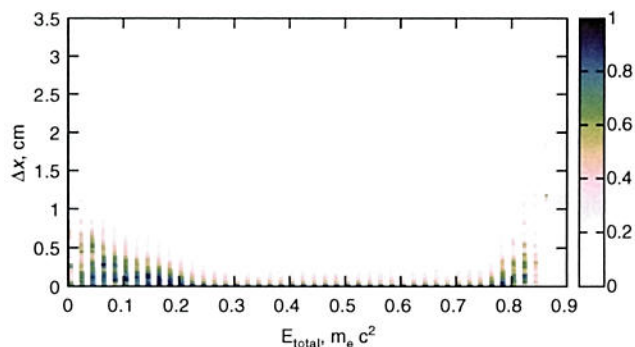


**Figure 7** Case C: histograms of  $|\Delta x|$  as a function of total deposited energy.

This figure shows a set of 1D histograms normalized to unity in maximum. A more detailed description can be found in the text.

The results presented in these figures indicate that, in order to decrease the blurring of the signals due to the secondary scattering, one can select from the full spectrum only these events for which the deposited energy is larger than  $0.2 m_e$  and smaller than  $0.7 m_e$ . For each of the studied cases, the broadest  $|\Delta x|$  distributions are observed for the energy deposition larger than the maximum energy deposition in the primary scattering ( $0.67 m_e$ ). In general, the largest spread of  $|\Delta x|$  is observed as expected for case C, for which the primary  $\gamma$  quantum can travel the longest distance along the scintillator. In this case, a scattering under small angles resulting in small energy depositions leads to the scattered  $\gamma$  quantum, which due to the relatively large energy can travel on the average large distance before the second scattering, which may again occur at most probably under a small angle with a small energy deposition. Therefore, in this case, the broad  $|\Delta x|$  distributions are observed also at the small values of the total deposited energy. The full energy spectra for all cases are presented in Figure 8.

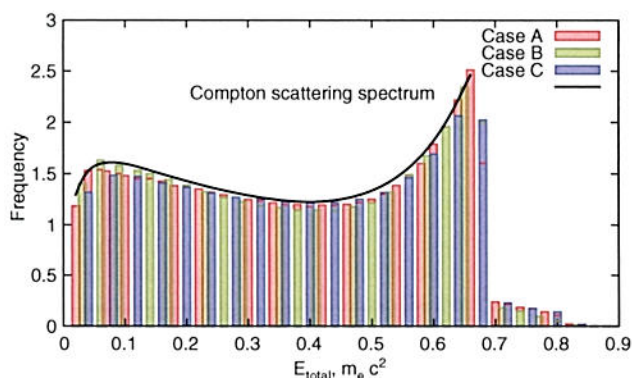


**Figure 8** Simulated spectra of the total energy deposited in the scintillator strip by annihilation  $\gamma$  quanta for cases A–C. The superimposed solid line shows the spectrum expected in the case of a single scattering.

## Distribution of time differences between subsequent interactions

The spatial distance of the first and subsequent interactions, along with their time difference, leads to the blurring of signal coming to the photomultipliers. The light signals are read out by photomultipliers on both edges of the strip; therefore, for one of them, the signal distortion by the secondary scattering will be much smaller than for the other one. This is because between the primary and secondary scatterings the  $\gamma$  quantum propagates toward one of the photomultipliers together with the primary light signal; therefore, the signal distortion in this photomultiplier will be smaller than in the other edge, where the delay between the primary and secondary light pulses is equal to

$$\Delta\tau = \frac{\Delta x}{c'} + \Delta t, \quad (6)$$

where  $\Delta x$  denotes the difference of the  $x$ -component of interactions' positions,  $\Delta t$  denotes their time difference, and  $c'$  stands for the effective velocity of light signal propagation through the scintillator. In this calculations,  $c' = 14 \text{ cm ns}^{-1}$  was used. The histogram of  $\Delta\tau$  (normalized to the PDF) is shown in Figure 9.

## Discussion and conclusions

The simulations of the scattering of annihilation  $\gamma$  quanta in a strip of polymer scintillator have been conducted. Such strips constitute the basic detection modules of the

newly proposed PET detector being developed by the J-PET Collaboration [5, 6]. An algorithm simulating the chain of Compton scatterings was elaborated and a series of simulations have been conducted for the scintillator strip with a cross-section of  $5 \times 20 \text{ mm}$ . The simulations were simplified due to the observation that for the energy range of interest the Compton scattering is dominant and the photoelectric and Rayleigh effects may be neglected. As a result, (i) the distributions of the multiplicity of interactions, (ii) the spatial distribution of interaction points as a function of the deposited energy, and (iii) the spectra of time differences between subsequent interactions have been determined. The results indicate that the secondary interactions occur only in the case of about 8% of the events and only 25% of these events take place in the distance larger than 0.5 cm. Also, the light signals produced at the primary and secondary interactions overlap with the delay, which is spread by about 40 ps (FWHM). Moreover, the analysis of histograms of the distance between subsequent interaction points as a function of the total deposited energy revealed that the blurring of signals due to the secondary interactions may be decreased by selecting from the full spectrum only these events for which deposited energy is larger than  $0.2 m_e$  and smaller than  $0.7 m_e$ .

**Acknowledgments:** We acknowledge technical and administrative support by M. Adamczyk, T. Gucwa-Ryś, A. Heczko, M. Kajetanowicz, G. Konopka-Cupiał, J. Majewski, W. Migdał, and A. Misiak and the financial support by the Polish National Center for Development and Research through Grant INNOTECH-K1/IN1/64/159174/NCBR/12, the Foundation for Polish Science through the MPD program, and the EU and MSHE Grant No. POIG.02.03.00-161 00-013/09.

### Conflict of interest statement

**Authors' conflict of interest disclosure:** The authors stated that there are no conflicts of interest regarding the publication of this article. Research funding played no role in the study design; in the collection, analysis, and interpretation of data; in the writing of the report; or in the decision to submit the report for publication.

**Research funding:** None declared.

**Employment or leadership:** None declared.

**Honorarium:** None declared.

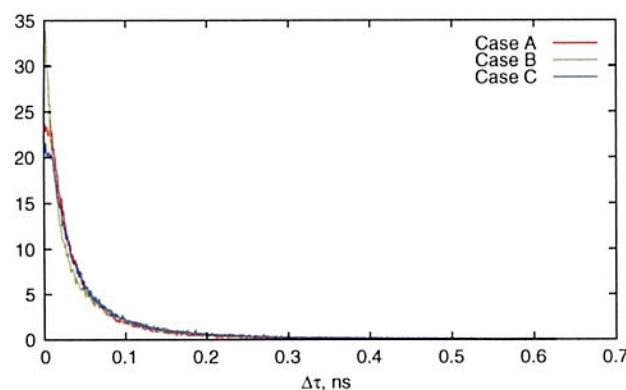


**Figure 9**  $\Delta\tau$  histogram (normalized to PDF) for cases A–C. The primary and secondary light signals overlap with a delay of about 40 ps (FWHM of the distribution).

Received October 28, 2013; accepted March 16, 2014

## References

1. Moskal P, Bednarski T, Białas P, Ciszewska M, Czerwiński E, Heczko A, et al. TOF-PET detector concept based on organic scintillators. In: Positron Emission Tomography in Research and Diagnostics Conference, May 16–19, 2012. Warsaw: Nuclear Medicine Review, 2012: C68–C69.
2. NIST XCOM (dynamic content). Photon cross-section database. Retrieved April 30, 2013 from <http://physics.nist.gov/PhysRefData/Xcom/Text/intro.html>.
3. Wolfram Research (dynamic content). Online integrator. Retrieved April 30, 2013 from <http://integrals.wolfram.com/index.jsp?expr=%28%281%2Bg%281-cos+x%29%29+%2B+1%2F+%281%2Bg%281-cos+x%29%29++sin^2+x+%29%2F%281%2Bg%281-cos+x%29%29^2+2+pi+sin+x+random=false>.
4. Silarski M. Polymer scintillators for PET produced commercially. Cracow: Jagiellonian University, 2012 (PET UJ Report nr 19/2012).
5. Moskal P, Salabura P, Silarski M, Smyrski J, Zdebik J, Zieliński M. Novel detector systems for the positron emission tomography. *Bio-Algorithms Med-Systems* 2011;7:73–8.
6. Moskal P, Bednarski T, Białas P, Ciszewska M, Czerwiński E, Heczko A, et al. Strip-PET: a novel detector concept for the TOF-PET scanner. *Nucl Med Rev* 2012;15:C68.